Earthquake Engineering & Structural Dynamics

WILEY

RESEARCH ARTICLE

Risk-Informed, Performance-Based Design of a Seismic Isolation System for a Nuclear Power Plant

Faizan Ul Haq Mir[1] | Ching-Ching Yu[2,3] | Mohamed M. Talaat[4] | Benjamin M. Carmichael[5] | Brandon M. Chisholm[5] | Andrew S. Whittaker[2]

[1]Department of Civil Engineering, Indian Institute of Technology Jammu, Jammu, Jammu and Kashmir, India | [2]Department of Civil, Structural, and Environmental Engineering, University at Buffalo, Buffalo, New York, USA | [3]TerraPower, Bellevue, Washington, USA | [4]Simpson Gumpertz & Heger, Oakland, California, USA | [5]Southern Company, Birmingham, Alabama, USA

Correspondence: Faizan Ul Haq Mir (mir.faizan@iitjammu.ac.in)

Received: 30 July 2024 | **Revised:** 28 February 2025 | **Accepted:** 2 April 2025

Funding: This work was supported by U.S. Department of Energy (DE-NE0008932).

Keywords: advanced nuclear reactors | performance-based design | risk analysis | seismic design | seismic isolation

ABSTRACT

A methodology to achieve a user-specified performance target for a seismic base-isolation system for a nuclear power plant (NPP) is presented and demonstrated. The isolation system, composed of both isolators and damping devices, is treated as a structure, system, and component (SSC) per US nuclear practice. Acceptable performance is defined as sufficient horizontal displacement capacity of the isolators and dampers to achieve a user-specified target performance goal (TPG). The methodology involves the generation of a seismic displacement demand curve for the isolation system, expressed as the mean annual frequency of exceedance (MAFE) of a horizontal displacement, and a fragility function for the isolation system. Information is presented on the derivation of an isolation system fragility function. The methodology is described via application to six isolation systems installed beneath an advanced NPP, founded on two different soil domains, and located at Clinch River in East Tennessee, USA.

1 | Introduction

Seismic isolation systems, comprised of isolators (also termed bearings) and damping devices (also termed dampers), have been widely used to substantially reduce seismic demands on buildings, bridges, and mission-critical infrastructure. The increase in total displacement associated with the reduction in acceleration can be substantially mitigated by the addition of damping devices installed at the level of the isolation interface. Seismic isolation systems have been implemented to protect assets across a wide range of sizes, from buildings and infrastructure to equipment and mechanical systems, and to small, priceless sculpture. Kammerer et al. [1] and Whittaker et al. [2] discuss applications of seismic base isolation to non-nuclear and nuclear facilities through late 2017. Applications to operating nuclear facilities are limited to the Cruas nuclear power plant in France (early 1980s), the Koeberg nuclear power plant in South Africa (early 1980s), a spent fuel pool at Le Hague in France, and emergency operations buildings at some Japanese nuclear power plants (e.g., Kashiwazaki-Kariwa, Fukushima Daiichi, Fukushima Daiini, and Onagawa). The Jules Horowitz research fission reactor and the ITER fusion reactor, both in Caderache, France, and under construction at the time of this writing, are being seismically isolated using synthetic rubber bearings like those adopted at Cruas and Koeberg.

Figure 1 illustrates the installation of a seismic base isolation system beneath an archetype reactor building, with isolators and dampers installed between the building's basement and its foundation. The figure defines terms used in the paper.

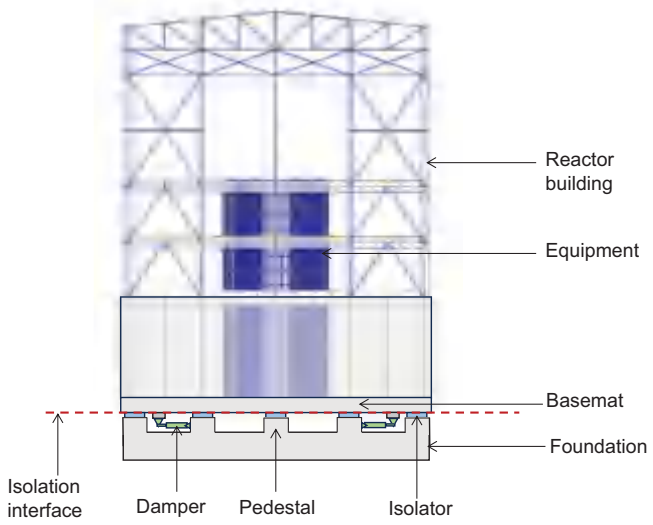

FIGURE 1 | Archetype isolated reactor building.

The US deployments of seismic isolation to buildings, bridges, and infrastructure have followed prescriptive rules presented in consensus standards such as ASCE/SEI Standard 7 [3] and the AASHTO Guide Specification [4], which require analysis, design, and testing for ground shaking attached to return periods of 2475 and 975 years, respectively, but without explicit calculations of seismic risk.

Because the US nuclear industry uses risk calculations to select a return period for design-basis earthquake shaking, a risk-informed, performance-based methodology (e.g., Stamatakos et al. [5]) is proposed in this paper for the analysis and design of seismic isolation systems for US nuclear power plants. The isolation system is treated as a structure, system, or component (SSC) per ASCE/SEI 43 [6] and ANS 2.26 [7], to which a seismic design category (SDC) is assigned, each with an associated target performance goal (TPG). The methodology is agnostic to reactor technology and power output, which will affect the selection of a SDC.

The mean annual frequency (MAF) of unacceptable performance, or the seismic risk (R), can be computed using Equation (1) [8], namely, by integrating a fragility function ($p_f(a)$) over a seismic hazard curve ($\lambda_H(a)$):

$$R = -\int p_f(a)\left(\frac{d\lambda_H(a)}{da}\right)da \tag{1}$$

where a is a demand parameter. The required performance of an isolation system is sufficient horizontal displacement capacity[1]. Accordingly, horizontal displacement is used as the demand parameter, requiring the isolation-system fragility function and the seismic hazard curve to be expressed in terms of this variable. Enough clearance around the isolated building must be provided to permit the isolated building to horizontally displace without impacting adjacent construction.

A fragility function for an isolation system is derived later in this paper and it is assumed to be a cumulative lognormal distribution defined by a median capacity (θ) and a logarithmic standard deviation (β). Figure 2a presents a sample fragility function for an isolation system, defined by θ = 250 mm and β = 0.35.

Seismic hazard curves are traditionally presented in terms of spectral acceleration at user-specified frequencies versus mean annual frequency of exceedance (MAFE): see Figure 2b for sample hazard curves that are used later in this paper. Because the demand parameter here is horizontal displacement, these curves must be transformed into a seismic displacement demand curve prior to calculating the seismic risk. A simple transformation from acceleration to displacement via angular frequency is not possible, unless the isolation system is linear and lightly damped, and most isolation systems are not. Two paths to generating a seismic displacement demand curve are presented later in this paper, with the recommended path in the body of the paper and the alternate in Appendix 1.

2 | Isolation Systems

An archetype reactor building, a hypothetical site, and six isolation systems are considered herein to demonstrate the process to achieve a user-specified TPG for a seismic isolation system. The reactor building, including its safety-class equipment, is loosely based on an early version of a fluoride salt-cooled reactor being developed by Kairos Power of Alameda, CA. The building is assumed to be sited in a region of moderate seismic hazard in the Central and Eastern United States (CEUS). The mass of the building is 8920 tons.

The six isolation systems considered here are summarized in Table 1. This list is by-no-means exhaustive, but it includes isolation systems comprising isolators and dampers available for possible deployment in the United States at the time of this writing. In Table 1, H1 and H2 are the principal horizontal axes of the building, and V denotes the vertical direction. Of the six systems, five provide horizontal (2D) isolation: (1) 2-s linear elastomeric (low damping, LDR) isolators with damping assumed equal to 5% of critical, (2) 2-s nonlinear single spherical sliding isolators, (3) 2-s linear elastomeric (LDR) isolators and uniaxial (1D) horizontal nonlinear fluid viscous dampers (FVDs), (4) 2-s nonlinear single spherical sliding isolators and 1D horizontal nonlinear FVDs, and (5) 3-s spherical sliding isolators. System 6 provides three-directional (3D) isolation. System 6 is identified as a 3D linear system herein and is composed of 3D machined- or coil-spring isolators and 3D viscoelastic dampers. Details about the mechanical properties of these isolation systems can be found in section 4 of Mir et al. [9] and the digital appendix provided with this paper.

The reactor building of Figure 1 is supported on 17 isolators, shown as black solid circles in Figure 3. This layout is used for the 2D (2H) and 3D (2H and 1 V) isolation systems introduced in Table 1. Supplemental horizontal 1D fluid viscous dampers, which are deployed in two of the six isolation systems, are located by the dashed green lines in Figure 3: four along each horizontal axis of the building. Supplemental vertical 1D fluid viscous dampers and 3D viscoelastic dampers, which are used in the 3D isolation system, are located adjacent to each of the 17 isolators.

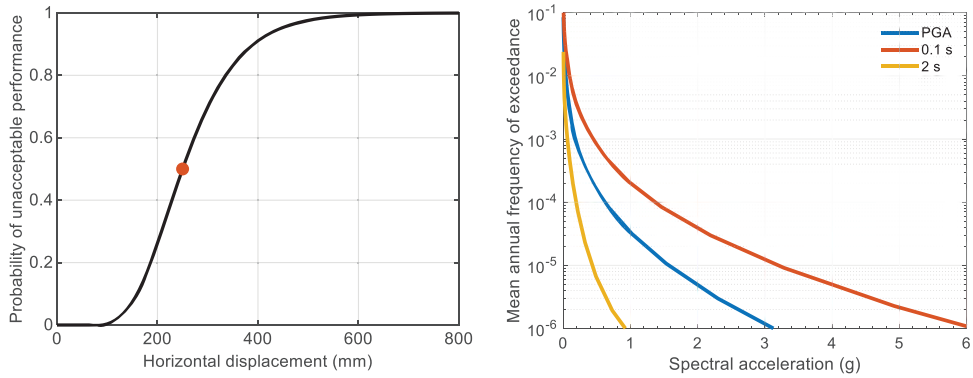

(a) isolation system fragility function (b) seismic hazard curve, 5% damping

FIGURE 2 | Inputs to a seismic risk calculation.

TABLE 1 | Isolators and dampers used in the six isolation systems for the reactor building, horizontal (H1, H2) and vertical (V) directions.

System	Isolation direction	Isolators		Dampers	
		H1, H2	V	H1, H2	V
1	2D	2-s linear	—	—	—
2	2D	2-s nonlinear	—	—	—
3	2D	2-s linear	—	1D nonlinear FVDs	—
4	2D	2-s nonlinear	—	1D nonlinear FVDs	—
5	2D	3-s nonlinear	—	—	—
6	3D	3D linear; 1.1 s for H and 0.4 s for V		3D viscoelastic dampers	

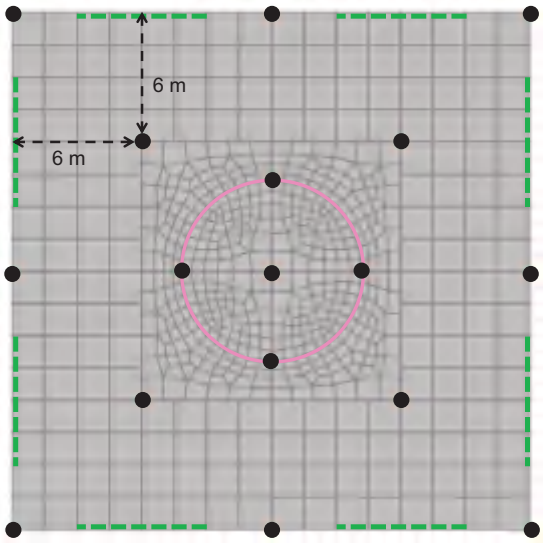

FIGURE 3 | Basemat of the reactor building, isolators (17) located by black solid circles and dampers (8) by dashed green lines.[2]

A two-degree-of-freedom (2DOF) model of the base-isolated reactor building in the horizontal plane is developed in the finite element program SAP2000 [10] to support the risk calculations. Figure 4 presents the 2DOF model: an oscillator comprised of a lumped mass of 8920 tons and one or two link elements representing all isolators and dampers in an isolation system. The two degrees of freedom are along the x (H1) and y (H2)

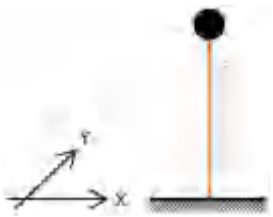

FIGURE 4 | Two-degree-of-freedom model; orange links used to simulate the isolation system.

axes. For calculating horizontal isolation-system displacements, the model assumes that the building is rigid, and the dynamic responses are characterized using one mode in each horizontal direction. (The assumption that the reactor building is rigid is reasonable because the reinforced concrete building envelope that surrounds the nuclear safety-class equipment is stiff, with lateral frequencies of 5 Hz and higher, with a ratio of building-to-isolation-system stiffness of more than 25. The perimeter steel braced frame shown in Figure 1 is stiff and lightweight, with frequencies also higher than 5 Hz.) Because the focus herein is the horizontal displacement response of the isolation system, a numerical model with two orthogonal horizontal degrees of freedom is sufficient for response-history analyses. (Past studies (e.g., Mosqueda et al. [11]) that addressed the effect of vertical shaking on the horizontal displacement response of isolated buildings concluded that varying axial loads had no meaningful effect.) The link elements modeling the isolation system are

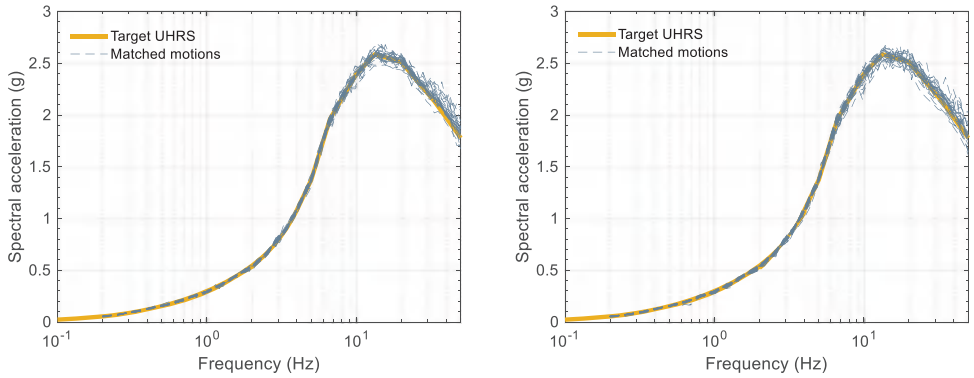

(a) *x*-direction (b) *y*-direction

FIGURE 5 | Response spectra of matched motions and UHRS for 25,000 years, Clinch River, BC soil, two components, 5% damping.

placed vertically in the model and have 6 degrees of freedom. The rotational degrees of freedom are restrained. The 2DOF model used here does not consider variability or uncertainty in isolation-system properties, which are addressed later in this paper via the isolation-system fragility function.

3 | Ground Motions for Dynamic Analysis

To demonstrate the risk-informed, performance-based design methodology, the reactor building is assumed to be sited at the East Tennessee Technology Park (ETTP) in Oak Ridge, Tennessee (TN), near Clinch River. The selected latitude-longitude pair for the site is (35.94°N, 84.40°W). Two different near-surface soil domains are considered to demonstrate the effect of soil conditions on the isolation-system displacement capacity required to achieve the TPG. The soft rock site (soil site) is represented by the boundary between site classes B and C (C and D) per ASCE/SEI Standard 7 [3], with an average shear wave velocity in the upper 30 m of the soil domain of 760 m/s (360 m/s). The TPG for the isolation system is assumed to be 4×10^{-5} to present the methodology.

To enable seismic analyses of the reactor building, seismic hazard curves, uniform hazard response spectra (UHRS), and ground motions for the Clinch River site are generated for the BC and CD soil domains using data provided by the United States Geological Survey [12]. The uniform hazard response spectra are developed for a return period of 25,000 years (= the reciprocal of the chosen TPG). Seed ground motion triplets are chosen based on a disaggregation of the seismic hazard at the site into magnitude-distance pairs. (Shaking consistent with the 25,000-year UHRS is referred to as TPG shaking hereafter.) The two-component seed motions are spectrally matched, per nuclear-industry practice, to the UHRS for BC and CD soils using RSPMatch2005 [13]. The two components of each matched-motion pair comply with the requirements of section 2.6.2 of ASCE/SEI Standard 4–16 [14] for statistical independence. Figure 5 presents the 5%-damped acceleration spectra of the matched motions and the UHRS in the two horizontal directions for BC soil. There are 30 matched motion spectra (gray) in each panel. Companion spectra for CD soil are presented in Mir et al. [9].

A displacement demand curve for an isolation system is generated by nonlinear response-history analysis for multiple intensities of ground shaking. The 2-s spectral acceleration (5% damped) hazard curve is chosen here for ground-motion scaling because longer period, 2D seismic isolation systems are the primary focus in this paper. Figure 6 presents the 2-s spectral acceleration seismic hazard curve for BC soil at the Clinch River site. The ticks on the vertical axis of the plot are in a base-10 log scale, termed *log scale* hereafter. The logarithm of the TPG is marked on the vertical axis of the figure and the corresponding spectral acceleration is marked as SA_{TPG} on the horizontal axis.

The terms *span* and *bins* are used in Figure 6 and in the discussion below. The term *span* refers to the range (or decades) of MAFE on the hazard curve (in log scale) considered in the analysis. The *span* is discretized into *bins*. A *span* of 4, centered on the TPG, and eleven *bins* of equal width in log space on the vertical scale, as shown in Figure 6, were used for analysis here, based on a sensitivity study involving combinations of span, bins, and isolation systems (see appendix D of Mir et al. [9]). Bin 6 is centered on the TPG. In Figure 6, the considered range of the vertical axis is the closed interval $[\log(TPG)—span/2, \log(TPG) + span/2] = [-2.39, -6.39]$, which corresponds to MAFEs equal to 4×10^{-3} and 4×10^{-7}, respectively. The boundaries of the eleven bins are defined by twelve equally spaced points in $[-2.39, -6.39]$, such that the width of each bin is 0.37 (= $span/11$ = 4/11) in log space[3]. The contribution of the hazard curve outside the interval $[\log(TPG)—span/2, \log(TPG) + span/2]$ is not significant relative to the TPG and is therefore ignored. (In this study, binning is conducted along the vertical axis. An alternative strategy involves employing the horizontal axis for binning, necessitating the establishment of bin limits based on the ground motion parameter. Using the vertical axis for binning in this application directly connects with the return periods on the earthquake shaking.)

The MAFE associated with the i^{th}-bin, corresponding to the center of the bin (i.e., the ordinate of the red dot), is denoted E^i, and the associated 2-s spectral acceleration is denoted SA^i. The thirty motions generated using spectral matching to the 25,000-year UHRS (TPG shaking) were amplitude scaled for the i^{th}-bin by a factor of SA^i/SA_{TPG}. The width of i^{th}-bin in linear space, ΔE^i, represents the mean annual frequency (MAF) for the bin containing SA^i. (The width of the i^{th}-bin in the log space is denoted $\Delta E^i_{\log}$ in Figure 6; and $\Delta E^i_{\log} = 0.37$ for all i.)

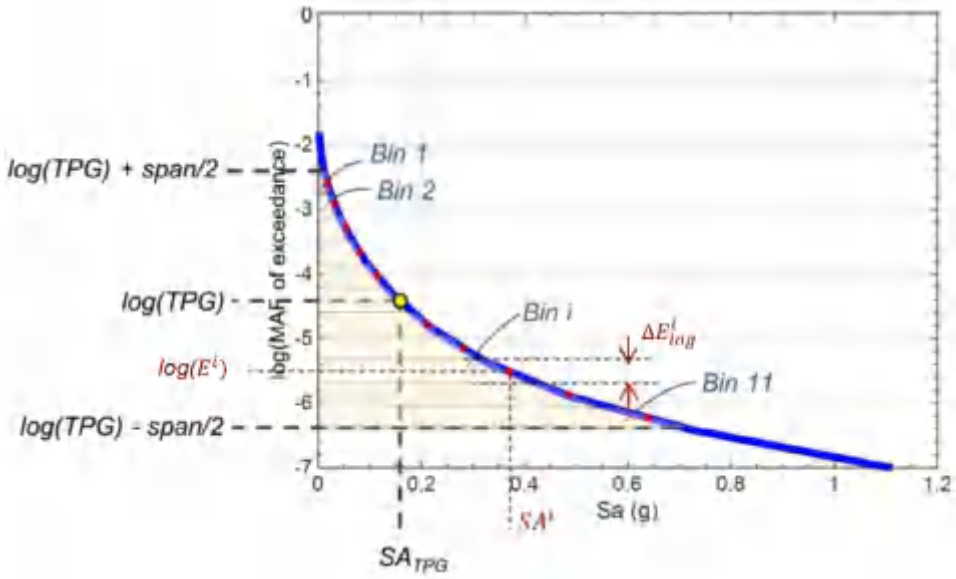

FIGURE 6 | 2-s spectral acceleration hazard curve, BC soil, calculation of scale factors for return periods other than 25,000 years, TPG = 4×10^{-5}.

4 | Generating a Displacement Demand Curve

A seismic horizontal displacement demand curve is determined by dynamic analysis of a 2DOF model of the isolated building for incremented levels of ground shaking. Best-estimate properties are used to define the force-displacement hysteresis of the isolation system. The displacement demand curve, which is specific to a user-selected isolation system, is generated in six steps, namely:

1. Generate uniform hazard response spectra (UHRS) for the site for geometric mean horizontal shaking for 11 return periods (i.e., reciprocal of MAFE) spanning 4 decades, centered on the TPG.
2. Generate 11 sets of ground motion acceleration time-series pairs, for each of the 11 return periods, that are spectrally matched to the geometric mean UHRS[4].
3. Analyze the two degree-of-freedom model of the user-selected seismic isolation system for each ground motion pair (H1, H2) in the set of 11 in a bin and calculate the mean maximum resultant horizontal displacement.
4. Repeat step 3 for all 11 bins.
5. Increase the 11 horizontal displacements from step 4, calculated using spectrally matched motions, by a factor of 1.2 to address the variability in (a) the horizontal components of ground motion, H1 and H2, around the geometric mean, and (b) the mechanical properties of the isolators and dampers. (The basis of the factor of the displacement multiplier of 1.2 is explained in the following section.).
6. Generate the displacement demand curve using the midpoint MAFE for each bin from step 1 (E^i) and the corresponding displacement from step 5.

Figure 7 presents the demand curves for BC and CD soils, and all six isolation systems. The choice of isolation system has a significant effect on the displacement demand curve, as evident in the figure.

5 | Deriving an Isolation System Fragility Function

Per Equation (1), the MAF of unacceptable performance of a seismic isolation system is computed by the convolution of its fragility function and a seismic horizontal displacement demand

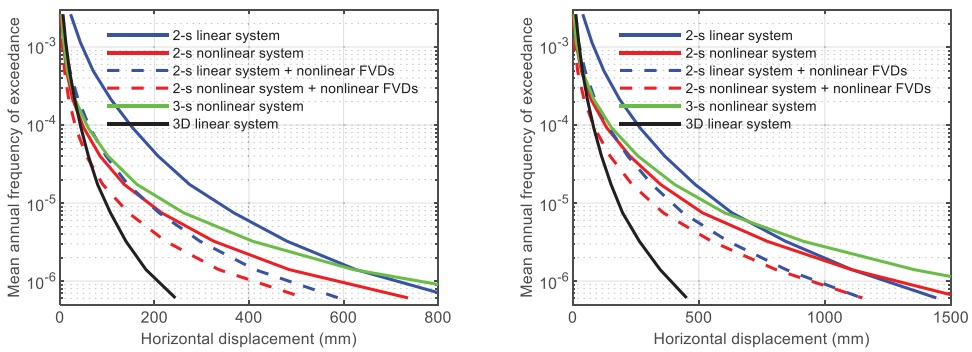

FIGURE 7 | Displacement demand curves, six isolation systems, Clinch River, BC and CD soils.

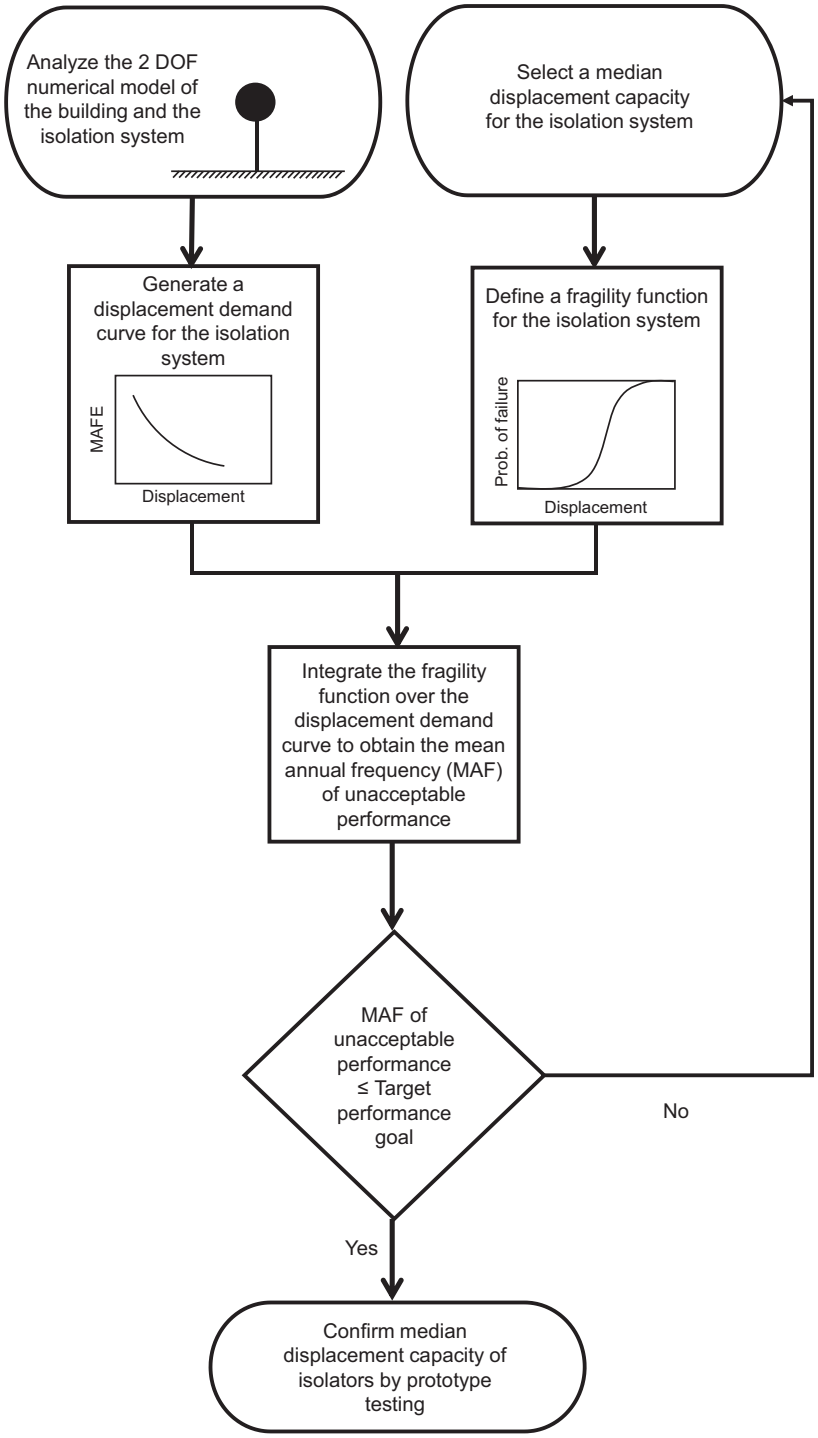

FIGURE 8 | Achieving a target performance goal for an isolation system, workflow diagram.

curve. The median displacement of the fragility function is adjusted until the MAF of unacceptable performance is equal to the user-specified TPG[5]. Figure 8 presents the workflow.

The logarithmic standard deviation of the isolation-system fragility function is given by

$$\beta = \sqrt{\beta_d^2 + \beta_c^2} \tag{2}$$

where β_d is the uncertainty in the displacement demand that is not accounted for in the seismic displacement demand curve and β_c is the uncertainty in the displacement capacity. Dispersions β_d and β_c are calculated using the variables listed in Table 2, which is adapted from EPRI [17], and are similar to the presentation in EPRI [18][6].

5.1 | Variability in Demand (β_d)

Dynamic analysis of a base-isolated building is more straightforward and accurate than that for a conventional nuclear power plant (NPP) structure because response is dictated by the behavior

TABLE 2 | Parameters affecting demand and capacity [17].

Demand	Capacity
1. Ground motion	8. Strength
2. Modeling	9. Inelastic energy absorption
3. Damping	
4. Mode combination	
5. Input time series	
6. Foundation-structure interaction	
7. Earthquake component combination	

of the seismic isolation system, whose materials (e.g., rubber, lead, and stainless steel) and devices are well characterized, and the manufacturing of isolators and dampers is of high quality. The isolation-system displacement response is accurately described using two horizontal modes, which is taken advantage of herein. Therefore, the demand-related discussion below focuses solely on the horizontal displacement response of the seismic isolation system.

Many of the variables listed in EPRI [17] do not apply to the fragility analysis of an isolation system; these are numbered 3 through 9 in Table 2. Descriptions of these variables can be found in section 3 of EPRI [17]. The damping ratio (energy dissipated per cycle, #3) of isolators and dampers is confirmed by prototype and production testing, variability is expected to be very small in production devices, based on US non-nuclear experience, and the force-displacement hysteresis (or damping) is included explicitly in the dynamic analysis. Importantly, since an isolation system will generally be composed of 10s to 100s of isolators and dampers, system variability will be smaller than that of an individual device. Uncertainty associated with modal combinations (#4) is negligible because isolation-system response is dominated by one mode in each horizontal direction. Variability in the input time series (#5) is explicitly accounted for in the probabilistic demand curve using the acceleration time series ensemble. The variability in foundation-structure interaction (#6) is not considered because soil-structure-interaction is of no importance for isolated nuclear structures because its frequency is well removed from that of the supporting soil domain [19]. Combining responses (#7) from shaking components (e.g., H1 and H2) is explicitly performed time step by time step and its variability is accounted for in the probabilistic demand curve. Variables numbered 8 and 9 in Table 2 are discussed later.

Variability in ground motion (#1) and modeling of isolator, damper, and structure (#2), bolded in Table 2, affect the horizontal displacement demand, and must be addressed. The accuracy of modeling of the isolation system is related to the identification of its mechanical properties and supported mass, and uncertainty in the fidelity of the model[7]. Accordingly, the dispersion in the displacement demand β_d is associated with four sources and is calculated as:

$$\beta_d = \sqrt{\beta_{gm}^2 + \beta_i^2 + \beta_m^2 + \beta_f^2} \tag{3}$$

where β_{gm}, β_i, β_m, and β_f are the dispersions in the displacement demand due to the uncertainty and/or variability in ground motion, mechanical properties of the isolation system, distribution of mass in the isolated superstructure, and model fidelity, respectively.

Dispersions are derived below for nonlinear systems, which include all isolation systems listed in Table 1, aside from System 1, which can be accurately modeled using a linear spring and a dashpot in parallel, with a damping coefficient that is independent of frequency, temperature, and displacement. Systems 2 and 6 of Table 1, which include 1D and 3D dampers, respectively, are nonlinear, noting that the response of the 3D viscoelastic damper of System 6 is dependent on frequency, temperature, and displacement. There are insufficient data from which to derive a default dispersion for linear systems, which will be smaller than those for nonlinear systems. The dispersions developed for nonlinear systems can be applied to linear systems.

5.1.1 | Derivation of Dispersions

Variability in isolator displacement response[8] due to ground motion is due to the difference between the distribution of earthquake shaking and the inputs used for dynamic analysis. Herein, ground motions are matched to a target UHRS, which is developed by probabilistic seismic hazard assessment and addresses both variability and uncertainty in the calculation of spectral demands at each annual frequency of exceedance.

The dispersion in the horizontal displacement response of the isolation system due to ground motion is computed by parsing β_{gm} into β_0 and β_{mm} as:

$$\beta_{gm} = \sqrt{\beta_0^2 + \beta_{mm}^2} \tag{4}$$

where β_0 is the dispersion associated with analysis using spectrally matched horizontal motions and β_{mm} is the additional dispersion due to variability in the two horizontal components around their geometric mean. Equation (3) can be rewritten as:

$$\beta_d = \sqrt{\beta_0^2 + \beta_{mm}^2 + \beta_i^2 + \beta_m^2 + \beta_f^2} \tag{5}$$

Two sources of data were used to develop β_0 and β_{mm}. Data generated in this study is used to determine β_0, building on information presented in Huang et al. [20, 21]. The data of Huang et al. [20, 21] is used to determine β_{mm}, for which the ratio of maximum to geometric mean spectral demands at longer periods had a median of 1.3 and a logarithmic standard deviation of 0.13. Those studies used 30 sets of ground motions per bin to ensure that the sample dispersion approximated the population dispersion.

Huang et al. [20, 21] considered three sites of very different seismic hazard: 1) Eastern United States (EUS), North Anna, Virginia, 2) Central and Eastern United States (CEUS), Vogtle, Georgia, and 3) Western United States (WUS), Diablo Canyon, California. The ground motions developed for analysis were consistent with a design response spectrum (DRS) and 150% DRS for an SDC-5 nuclear power plant. All the input motions included

TABLE 3 | Data from table III of Huang et al. [21], Eastern United States, North Anna.

	DRS shaking								150% DRS shaking							
Model	θ_{G0} (mm)	θ_{M0} (mm)	θ_{M1} (mm)	θ_{M2} (mm)	β_{G0}	β_{M0}	β_{M1}	β_{M2}	θ_{G0} (mm)	θ_{M0} (mm)	θ_{M1} (mm)	θ_{M2} (mm)	β_{G0}	β_{M0}	β_{M1}	β_{M2}
LR_T2Q3	31	35	35	35	0.10	0.12	0.12	0.13	43	50	50	50	0.13	0.13	0.14	0.14
LR_T3Q3	35	40	40	40	0.11	0.13	0.13	0.14	50	58	58	58	0.13	0.17	0.17	0.18
LR_T4Q3	37	43	43	43	0.11	0.14	0.15	0.15	52	63	63	62	0.12	0.17	0.17	0.17
FP_T2Q3	9.4	11	11	11	0.18	0.25	0.24	0.25	18	23	23	23	0.19	0.23	0.23	0.25
FP_T3Q3	10	12	12	12	0.20	0.24	0.24	0.24	19	24	24	24	0.20	0.23	0.23	0.24
FP_T4Q3	11	13	13	13	0.21	0.23	0.23	0.24	20	25	25	25	0.21	0.23	0.23	0.25
LDR_T2	61	70	70	69	0.12	0.10	0.10	0.10	92	105	105	104	0.12	0.10	0.10	0.10
LDR_T3	63	72	72	72	0.11	0.10	0.10	0.10	94	109	109	108	0.11	0.10	0.10	0.10
LDR_T4	63	73	73	73	0.12	0.12	0.12	0.12	95	110	110	110	0.12	0.12	0.12	0.12

Abbreviations: FP = Friction Pendulum; LDR = low damping rubber, LR = lead-rubber, Q* = zero-displacement force-intercept normalized by supported weight, T* = * second period.

TABLE 4 | Data from table V of Huang et al. [21], Central and Eastern United States, Vogtle.

	DRS shaking								150% DRS shaking							
Model	θ_{G0} (mm)	θ_{M0} (mm)	θ_{M1} (mm)	θ_{M2} (mm)	β_{G0}	β_{M0}	β_{M1}	β_{M2}	θ_{G0} (mm)	θ_{M0} (mm)	θ_{M1} (mm)	θ_{M2} (mm)	β_{G0}	β_{M0}	β_{M1}	β_{M2}
LR_T3Q3	289	349	348	347	0.13	0.18	0.18	0.19	467	558	557	555	0.12	0.15	0.15	0.16
LR_T3Q6	204	264	263	263	0.16	0.24	0.23	0.24	368	456	455	454	0.15	0.21	0.21	0.22
LR_T4Q3	227	274	274	274	0.13	0.20	0.20	0.20	352	425	426	427	0.11	0.18	0.18	0.18
LR_T4Q6	195	238	238	238	0.15	0.23	0.23	0.23	309	373	374	374	0.16	0.23	0.23	0.23
FP_T3Q3	246	303	303	303	0.14	0.20	0.19	0.20	433	523	523	523	0.12	0.15	0.15	0.15
FP_T3Q6	140	190	190	189	0.21	0.30	0.30	0.31	308	391	391	391	0.18	0.25	0.24	0.25
FP_T4Q3	193	240	240	240	0.15	0.22	0.22	0.22	325	403	403	403	0.12	0.19	0.19	0.19
FP_T4Q6	128	168	168	168	0.20	0.29	0.28	0.29	255	319	319	319	0.18	0.26	0.25	0.26

Abbreviations: FP = Friction Pendulum, LR = lead-rubber, Q* = zero-displacement force-intercept normalized by supported weight, T* = * second period.

two horizontal and one vertical components: see Huang et al. [20, 21] for details.

The Huang et al. studies utilized ground motions matched to a geometric mean UHRS. Thirty seed ground motion triplets were first selected from recorded ground motions in the PEER database. The two horizontal components in the triplet, H1 and H2, were then separately matched to the target geometric mean UHRS, producing two different acceleration times series: the G0 motions introduced next.

Huang et al. generated four datasets: (1) G0, spectrum compatible ground motions, best estimate model of the isolation system, (2) M0, maximum–minimum (max–min) ground motions, best estimate model of the isolation system, (3) M1, max–min ground motions, varied mechanical properties of the isolation system (±10% of best estimate), and (4) M2, max–min ground motions, varied mechanical properties of the isolation system (±20% of best estimate). The max–min ground motions for analysis set M0, M1, and M2 were generated by Huang et al. using maximum direction spectra (see appendix A of Mir et al. [9] for details).

Table 3 through Table 5 present the median displacements and logarithmic standard deviations, extracted from Huang et al. [21], for the three sites, different isolation systems, DRS shaking and 150% DRS shaking, together with references to specific tables in that paper. (The subscripts to θ and β in these tables denote the analysis sets.)

5.1.1.1 | Derivation of β_0. The maximum dispersion in the horizontal displacement response of an isolation system for the G0 dataset, computed using data from Table 3 through Table 5, is 0.24 for the nonlinear systems: see the highlighted cell in Table 5.

Analysis of the data generated as part of this study is focused on one site, two soil conditions (BC and CD), and six horizontal isolation systems (per Table 1). The analysis herein utilized a broader range of earthquake shaking than that considered in Huang et al. [21], but also used spectrally matched motions, and yielded a slightly greater maximum dispersion, as explained next.

As described previously, seismic hazard curves are parsed into 11 bins spanning 4 decades in MAFE. Dynamic analysis is

TABLE 5 | Data from table X of Huang et al. [21], Western United States, Diablo Canyon.

Model	DRS shaking								150% DRS shaking							
	θ_{G0} (mm)	θ_{M0} (mm)	θ_{M1} (mm)	θ_{M2} (mm)	β_{G0}	β_{M0}	β_{M1}	β_{M2}	θ_{G0} (mm)	θ_{M0} (mm)	θ_{M1} (mm)	θ_{M2} (mm)	β_{G0}	β_{M0}	β_{M1}	β_{M2}
LR_T2Q3	488	572	573	576	0.10	0.13	0.13	0.14	792	932	932	936	0.09	0.12	0.12	0.13
LR_T2Q6	401	473	473	472	0.14	0.20	0.20	0.21	678	797	797	798	0.12	0.16	0.16	0.17
LR_T2Q9	338	404	404	405	0.19	0.25	0.25	0.25	595	703	703	702	0.14	0.21	0.21	0.21
LR_T3Q6	494	584	585	585	0.19	0.26	0.25	0.25	862	1039	1039	1041	0.18	0.22	0.22	0.22
LR_T3Q9	404	471	472	472	0.20	0.28	0.28	0.28	729	863	864	865	0.20	0.26	0.26	0.26
LR_T4Q9	418	493	493	495	0.21	0.29	0.29	0.29	779	951	951	950	0.19	0.24	0.24	0.24
FP_T2Q3	492	571	571	572	0.11	0.14	0.14	0.14	819	953	953	953	0.11	0.13	0.13	0.13
FP_T2Q6	392	461	461	461	0.15	0.22	0.21	0.22	686	800	801	801	0.13	0.17	0.17	0.17
FP_T2Q9	321	385	385	384	0.21	0.26	0.26	0.27	593	697	697	697	0.16	0.22	0.22	0.22
FP_T3Q6	471	555	556	557	0.21	0.28	0.27	0.28	852	1006	1006	1007	0.18	0.23	0.23	0.23
FP_T3Q9	374	442	443	443	0.23	0.29	0.29	0.30	707	832	833	834	0.21	0.28	0.27	0.27
FP_T4Q9	382	462	462	463	**0.24**	0.31	0.31	0.31	756	925	925	928	0.20	0.24	0.23	0.24

Abbreviations: FP = Friction Pendulum; LR = lead-rubber, Q* = zero-displacement force-intercept normalized by supported weight, T* = * second period.

TABLE 6 | Values of β_0 for isolation systems 1 through 6 of Table 1.

	Isolation system					
	1	**2**	**3**	**4**	**5**	**6**
BC soil	0.10	0.21	0.17	0.19	0.20	0.13
CD soil	0.10	0.22	0.19	0.28	0.24	0.17

performed for each ground motion pair (GM 1 to 30) in each bin to compute a maximum resultant horizontal displacement for isolation systems 1 through 6 in Table 1. The logarithmic standard deviation of the maximum resultant horizontal displacement is calculated for each bin. The average of the values in bins 5 through 8, is reported in Table 6. The dispersions for bins 1 through 4 are set aside because (a) the displacements are very small and of no significance to the risk calculation, and (b) production testing of isolators and dampers will preclude device failure at small displacements. The dispersions for bins 9, 10, and 11 are set aside because (a) the risk contributions are small for the associated annual frequency of exceedance (AFE), and (b) the values are smaller than those in the mid-range of the 11 bins, for the nonlinear systems. (See the annex to appendix C in Mir et al. [9] for more details.) Dispersions are listed for BC and CD soils in Table 6. The dispersions are the lowest for the lightly damped linear system (1) and highest for the nonlinear systems (2, 4, and 5). The dispersions for the heavily damped linear system (3) fall *midway* between those for the lightly damped linear and the nonlinear systems.

Based on the data presented in Table 6, and in the absence of project-specific calculations, β_0 is set equal to 0.28.

5.1.1.2 | Derivation of β_{mm} and β_i. Huang et al. [20, 21] characterized the variability in the horizontal displacement response of an isolation system due to both ground motion orientation and the mechanical properties of the isolation system: the M2 dataset.

The mechanical properties of the isolation systems considered by Huang et al. were allowed to vary by up to 20% from the values used for analysis and design, which is the limit set in section 9.2.2.1 of ASCE/SEI 43–19 [6]. The mechanical properties of the isolation system were assumed to be normally distributed with a coefficient of variation (i.e., the ratio of the standard deviation to the mean) of 0.10 [20].

The additional dispersion introduced by using max-min components of horizontal ground shaking for analysis (instead of spectrally matched components) and consideration of variability in the mechanical properties of the isolation system is computed using the data presented in Tables 3–5 for the nonlinear systems. For each row in these tables, the value of $\sqrt{\beta_{M2}^2 - \beta_{G0}^2}$ is calculated for DRS and 150% DRS shaking. The average of the 52 values is 0.14, and it partially accounts for $\sqrt{\beta_{mm}^2 + \beta_i^2}$, with the remainder addressed via β_r, as discussed next.

5.1.1.3 | Adjustment to Mean Displacement Demand and Derivation of Associated Dispersion, β_r. The analysis performed in this paper is analogous to analysis set G0 per Huang et al. [21], that is, analysis of a best estimate model of an isolation system using ground motions spectrally matched to a geometric mean spectrum. Accordingly, adjustments are made to the displacement demand curve, based on the results of response-history analysis using spectrally matched motions, to partly account for the variability in ground shaking around the geometric mean and in the properties of the isolation system. The remaining variability is addressed via the logarithmic standard deviation assigned to the fragility function.

The ratio of θ_{M2}/θ_{G0} for DRS and 150% DRS was calculated for all isolation systems and sites considered in the Huang et al. studies

using data presented in Tables 3–5. The average value of the ratio is 1.2. Accordingly, the ordinates of the seismic displacement demand curve computed using spectrally matched motions are increased by a factor of 1.2 in step 5 of the six-step process for generating a displacement demand curve. This factor addresses variability in ground shaking around the geometric mean and in the properties of the isolation system. The logarithmic standard deviation of the distribution of the ratio, β_r, is 0.05, and it is included in the fragility function as follows:

$$\beta_d = \sqrt{\beta_0^2 + \beta_{mm}^2 + \beta_i^2 + \beta_m^2 + \beta_f^2} = \sqrt{\beta_0^2 + [(\beta_{M2}^2 - \beta_{G0}^2) + \beta_r^2] + \beta_m^2 + \beta_f^2} \quad (6)$$

5.1.1.4 | Derivation of Mass Uncertainty, β_m. In-service differences from design assumptions, including the mass of the isolated superstructure and its distribution in plan, could alter the horizontal displacement response of an isolation system. However, the changes are expected to be very small because (a) much of the reactor building mass is reinforced concrete, for which the as-built construction should closely follow the design drawings, (b) the masses of large pieces of equipment will be included in the numerical model used for analysis, and (c) the isolation system will be designed to minimize torsional response. The dispersion in the displacement response associated with uncertainty in the distribution of the mass of the isolated superstructure, β_m, is assumed to be 0.05.

5.1.1.5 | Derivation of Model Fidelity Uncertainty, β_f. Per section 5.4.3.2 of EPRI [18], model fidelity uncertainty should be in the range of 0.05 to 0.15, noting that the "…former value (= 0.05) is applicable to structures whose responses are dominated by fundamental modes with simple mode shapes…" Because the response of a seismically isolated building will be dominated by its isolated modes, each with simple shape, β_f is set here to the bottom of the range, namely, 0.05.

5.1.1.6 | Recommendation for β_d. The uncertainty in demand, β_d, per Equation (6) is

$$\beta_d = \sqrt{\beta_0^2 + (\beta_{M2}^2 - \beta_{G0}^2) + \beta_r^2 + \beta_m^2 + \beta_f^2} = \sqrt{0.28^2 + (0.14^2) + 0.05^2 + 0.05^2 + 0.05^2} = 0.33$$

5.2 | Variability in Capacity

The two variables associated with capacity in Table 2 are strength and inelastic energy absorption (or damping). These variables were proposed for conventional reinforced concrete nuclear construction and not for seismically isolated nuclear structures.

The capacity of a seismic isolator and/or a damper, measured in terms of its force-displacement hysteresis, is confirmed by prototype testing of each type and size of device planned for construction, and by production testing of every device prior to shipment to the construction site. A lower bound on median capacity is established by prototype testing. There may be device-to-device variability, but for an isolation system which is comprised of many devices, the system-level variability is expected to be negligible, and so β_c is set equal to 0.05. Variations in mechanical properties are addressed in β_i above.

5.3 | Composite Dispersion, β

The value of the composite dispersion per Equation (2) for all isolation systems, in lieu of project- and site-specific calculations, is:

$$\beta = \sqrt{\beta_d^2 + \beta_c^2} = \sqrt{0.33^2 + 0.05^2} = 0.34$$

The recommended default value for β is based on the calculation above and rounded to the nearest 0.05, namely 0.35. The calculations presented hereafter use β= 0.35 for all sites and isolation systems, noting that project- and site-specific derivations of dispersions, such as those presented in this section would likely support the use of a smaller value for (a) lightly damped linear isolation systems, and (b) nonlinear systems on firm soil or rock sites. (Project-specific estimates of β_0 should be made with results of analysis using 30 sets of ground motions.)

6 | Performance Calculations

Figure 9 identifies the two key parts of one performance calculation. Figure 9a presents the displacement demand curve for isolation system 3 and BC soil, determined using the six steps presented in section 4. Figure 9b presents two isolation-system fragility functions, both with β =0.35, and median displacement capacities of 200 and 250 mm, respectively, representative of two candidate isolation systems.

The displacement demand curve of Figure 9a and the fragility functions of Figure 9b are discretized into 50 increments of horizontal displacement. Integrating the fragility functions of Figure 9b over the displacement curve of Figure 9a per Equation (1) results in annual frequencies of 1.1×10^{-5} and 6.3×10^{-6}. Increasing the median displacement capacity from 200 to 250 mm reduces the risk, which is an expected outcome. Figure 9c presents the contributions to the total risk by displacement bin for the two isolation systems.

The process of integrating the fragility function over the displacement demand curve is repeated for different values of the median displacement capacity. The median displacement that achieves the TPG is denoted D_{50}. Table 7 presents the required median displacement (D_{50}) for each of the six isolation systems to achieve the TPG of 4×10^{-5} (= 1/25,000 years). The values of D_{50} vary significantly for a given TPG because the displacement demand curves are different.

7 | Minimum Clearance to Adjacent Construction

Seismic isolators and dampers are produced using stringent controls on materials and manufacturing, with quality confirmed by (a) prototype testing of three units of each type and size for seismic demands consistent with the horizontal displacement

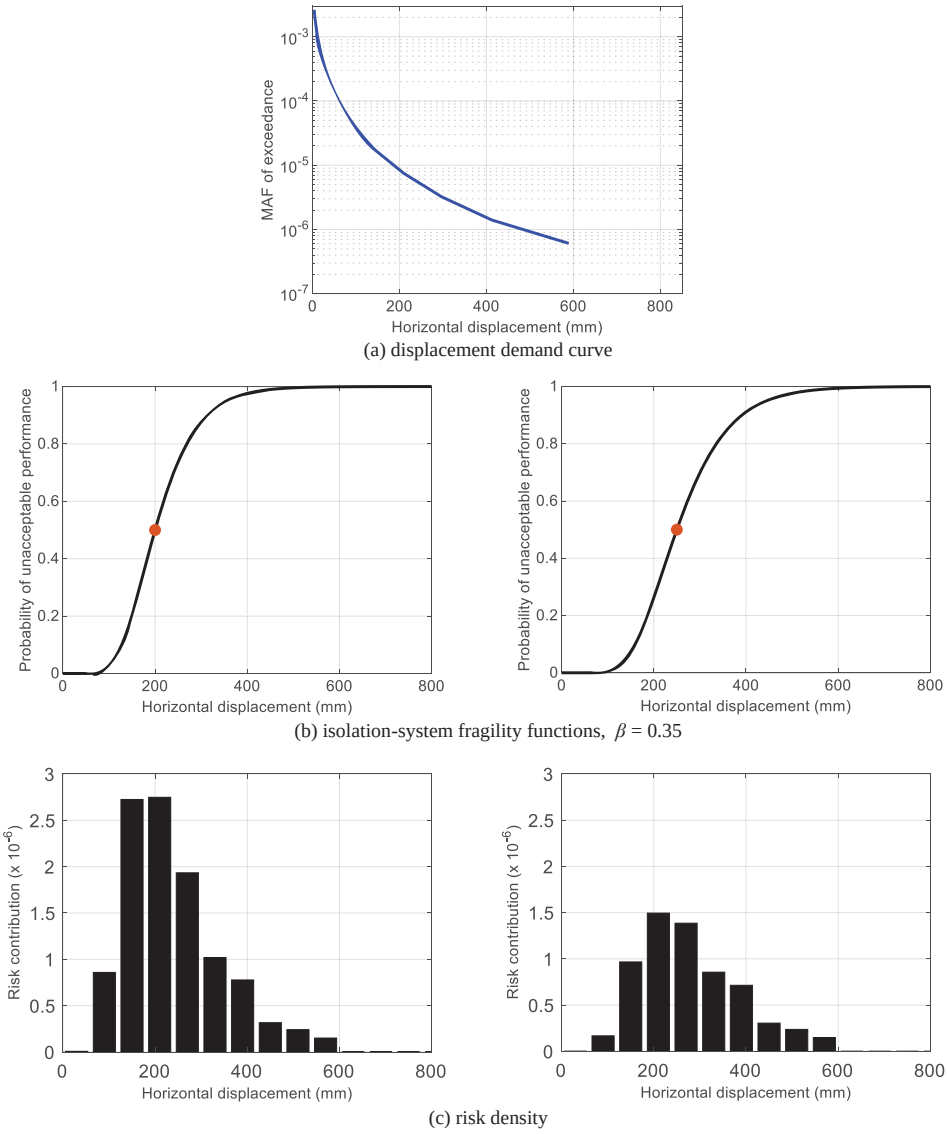

FIGURE 9 | Steps toward achieving a target performance goal: 2-s linear isolation system with supplemental nonlinear FVDs, Clinch River, BC soil.

TABLE 7 | Required median displacement capacity, D_{50}, to achieve a TPG of 4×10^{-5}, Clinch River, BC, and CD soils.

Isolation system per Table 1		Median displacement capacity, D_{50} (mm)	
		BC soil	CD soil
1	2-s linear system	242	424[a]
2	2-s nonlinear system	94	248
3	2-s linear system + nonlinear FVDs	110	244
4	2-s nonlinear system + nonlinear FVDs	62	162
5	3-s nonlinear system	112	284
6	3D linear system, $T_{iso,h}$ =1.1 s	70	132[a]

[a]Likely impractical, with another isolation solution needed.

D_{50}, and (b) production testing of all units to a horizontal displacement consistent with design basis (DB) shaking (See section 6 of Mir et al. [9] for details.). Accordingly, the variability in isolator and damper properties is more narrowly constrained than in conventional materials for building construction.

For a seismic isolation system with a displacement capacity defined by a median value D_{50} and a variability in capacity characterized by a logarithmic standard deviation of 0.05, as noted above, a clearance of $\pm 1.15 D_{50}$ between an isolated building and any adjacent construction along both horizontal axes is sufficient to ensure, with 99% confidence[9], that no impact will

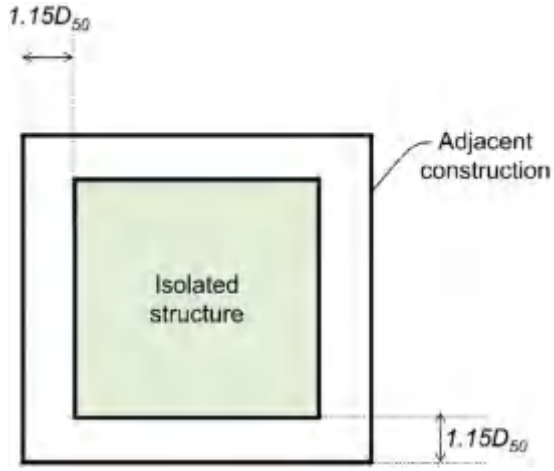

FIGURE 10 | Horizontal clearance around a seismically isolated nuclear power plant.

occur. Accordingly, the minimum clearance between an isolated building and any adjacent construction should be $1.15D_{50}$, as shown in Figure 10.

8 | Summary and Recommendations

A procedure to achieve a TPG for a seismic base isolation system in a NPP was described and then implemented using an archetype reactor building, one site, two soil domains, and six isolation systems. The procedure is agnostic to reactor technology and size, and the choice of 2D and 3D seismic isolation system. Because the isolation system is treated as an SSC per ASCE 43 [6] and ANS 2.26 [7], the procedure could be used to design an isolation system supporting safety-related equipment inside a reactor building, but the displacement demand curve would have to be developed by analysis of a model of the reactor building that includes explicit representation of the isolated equipment. The approach illustrated in this paper is compatible with current and proposed NRC licensing frameworks, namely, Part 50 [22], Part 52 [23], and the proposed language for Part 53 [24], of the Code of Federal Regulations.

The required performance of an isolation system for a nuclear power plant is sufficient horizontal displacement capacity to achieve the TPG. The required median displacement capacity is calculated using a seismic displacement demand curve and a logarithmic standard deviation for the isolation system fragility curve. An approach to define the seismic hazard range of interest and to subdivide it into bins to enable scaling of ground motions for dynamic analysis is presented. A procedure to generate a seismic displacement demand curve from the results of response-history analyses is described. Results of response-history analyses generated in this study for six isolation systems, two soil types, and one site are used, together with results from a prior study, to derive the logarithmic standard deviation (= 0.35) that should be used to define a fragility function for an isolation system in the absence of project- and site-specific calculations. The minimum required horizontal clearance between the isolated building and any adjacent construction is $1.15D_{50}$.

Acknowledgments

The authors thank the US Department of Energy for funding the writing of the topical report on the seismic isolation of advanced nuclear reactors under Award DE-NE0008932 to Southern Nuclear Development, LLC. The views and opinions of the authors expressed herein do not necessarily state or reflect those of the United States Government, TerraPower, Simpson Gumpertz & Heger, Southern Company, Indian Institute of Technology Jammu, or the University at Buffalo.

Data Availability Statement

The data that support the findings of this study are openly available in DesignSafe at https://doi.org/10.17603/ds2-15y1-dg79.

Endnotes

[1] For a 3D isolation system, vertical displacement must also be addressed, but it is assumed here that such movement is not constrained.

[2] Appropriate nodal connectivity in the basemat mesh is achieved using the *area edge constraint* command in SAP2000.

[3] The bins have unequal width in linear space. Consider bins 1 and 2. Bin 1 is bounded by −2.39 and −2.76 on the vertical axis in the log space, and bin 2 is bounded by −2.76 and −3.12, such that both bins have a width of 0.37 along the vertical axis in log space. The widths of bins 1 and 2 in linear space are $\Delta E^1 = 2.3 \times 10^{-3}$ ($= 10^{-2.39}$–$10^{-2.76}$) and $\Delta E^2 = 9.8 \times 10^{-4}$ ($= 10^{-2.76}$–$10^{-3.12}$), respectively.

[4] Eleven sets of motions provide a stable estimate of the median displacement in each bin, as adopted in section 5.2.2 of FEMA P-58-1 [15] for intensity-based assessments and documented in appendix C.3 of Huang et al. [16] Herein, 30 sets are used because (a) the ground motions were available from a prior study, and (b) 30 sets of motions are used in a later section to compute dispersions in each bin, which are then used to develop a default value of the logarithmic standard deviation for isolation-system fragility functions.

[5] The median displacement capacity of an isolator and/or a damper is confirmed by prototype testing (see section 6 of Mir et al. [9]). Given the acceptance criteria used for prototype testing, which does not permit device failure, median capacity will be underestimated by prototype testing, and perhaps substantially. Further, the failure of one isolator and/or damper does not compromise the integrity of the isolation system, and so the median capacity of an isolation *system*, as judged by prototype testing of individual isolators and dampers, is conservatively biased, with the resultant risk being overestimated.

[6] The 2018 EPRI report [18] consolidates the 1994 EPRI report [17] and other resource documents, presenting state-of-the-art methods for developing seismic fragilities in probabilistic risk assessments. EPRI [18] incorporates updated methods and corrections from EPRI [17].

[7] Uncertainty in fidelity of the model addresses the uncertainty in the model itself rather than its parameters: mode shape uncertainty per EPRI [18].

[8] Variability in the vertical-to-horizontal V/H ratio per EPRI [18], which supersedes the recommendations of EPRI [17], is not considered here because it does not affect the horizontal displacement response of an isolation system.

[9] At a displacement of $1.15D_{50}$, the cumulative distribution function of a lognormal distribution with median D_{50} and logarithmic standard deviation of ξ equals $\Phi((\ln(1.15D_{50}) - \ln(D_{50}))/\xi)$, where Φ denotes the cumulative distribution function (CDF) of a normal distribution $\Phi((\ln(1.15D_{50}) - \ln(D_{50}))/0.05) = \Phi(2.79) = 0.99$.

[10] Reliable information on exceedance frequencies is not available outside this range.

[11] The value of β = 0.18 (for approach A2) could be rounded to the nearest 0.05 per approach A1, namely, to 0.20, but 0.18 is used for the calculations presented herein.

References

1. A. M. Kammerer, A. S. Whittaker, and M. C. Constantinou, *Technical Considerations for Seismic Isolation of Nuclear facilities, NUREG/CR-7253 (ML19050A422)* (US Nuclear Regulatory Commission (NRC), 2019).

2. A. S. Whittaker, P. Sollogoub, and M.-K. Kim, "Seismic Isolation of Nuclear Structures: Past, Present, and Future," *Nuclear Engineering and Design* 338 (2018): 290–299.

3. American Society of Civil Engineers (ASCE), *Minimum Design Loads and Associated Criteria for Buildings and Other Structures* (ASCE/SEI 7–22, 2022).

4. American Association of State Highway and Transportation Officials (AASHTO), *Guide Specifications for Seismic Isolation Design*, 4th ed., American Association of State Highway and Transportation Officials, Washington, D.C. (2014).

5. J. Stamatakos, B. Dasgupta, O. Pensado, N. Chokshi, R. Budnitz, and M. Ravindra, "Proposed Enhancements to the Risk-Informed and Performance-Based Regulatory Framework for Seismic Hazard Design at NRC-Regulated Nuclear Power Plants," *Nuclear Science and Engineering* 197, no. 11 (2023): 2743–2750.

6. American Society of Civil Engineers (ASCE), Seismic Design Criteria for Structures, Systems, and Components in Nuclear Facilities (ASCE/SEI 43-19, 2021).

7. American Nuclear Society (ANS), Categorization of Nuclear Facility Structures, Systems, and Components for Seismic Design (ANSI/ANS-2.26-2004 (R2017), 2017).

8. R. McGuire, Seismic Hazard and Risk Analysis, *MNO-10* (Earthquake Engineering Research Institute, 2004).

9. F. U. H. Mir, C.-C. Yu, B. M. Carmichael, B. M. Chisholm, J. Redd, M. M. Talaat, C. Bolisetti, and A. S. Whittaker, Guidelines for Implementing Seismic Base Isolation in Advanced Nuclear Reactors, *MCEER-24-0001, Rev 1* (University at Buffalo, 2025).

10. Computers and Structures (CSI), SAP2000 Version 22.1.0. (2020).

11. G. Mosqueda, A. S. Whittaker, and G. L. Fenves, "Characterization and Modeling of Friction Pendulum Bearings Subjected to Multiple Components of Excitation," *Journal of Structural Engineering* 130, no. 3 (2004): 433–442.

12. United States Geological Survey (USGS), Hazard Curves for the 2018 Update of the U.S. National Seismic Hazard Model (2018), https://www.sciencebase.gov/catalog/item/5d559795e4b01d82ce8e3fef.

13. J. Hancock, J. Watson-Lamprey, N. A. Abrahamson, et al., "An Improved Method of Matching Response Spectra of Recorded Earthquake Ground Motion Using Wavelets," *Journal of Earthquake Engineering* 10, no. spec01 (2006): 67–89.

14. American Society of Civil Engineers (ASCE), Seismic Analysis of Safety-Related Nuclear Structures and Commentary (ASCE/SEI 4–16, 2017).

15. Federal Emergency Management Agency (FEMA), Seismic Performance Assessment of Buildings, Volume 1 - Methodology (FEMA P-58-1, 2012).

16. Y.-N. Huang, A. S. Whittaker, and N. Luco, Performance Assessment of Conventional and Base Isolated Nuclear Power Plants for Earthquake and Blast Loadings, *MCEER-08-0019* (University at Buffalo, 2008).

17. Electric Power Research Institute (EPRI), Methodology for Developing Seismic Fragilities, *TR-103959* (1994).

18. Electric Power Research Institute (EPRI), Seismic Fragility and Seismic Margin Guidance for Seismic Probabilistic Risk Assessments, *3002012994* (2018).

19. K. M. Lal, A. S. Whittaker, S. Vahdani, B. D. Kosbab, K. Shirvan, and S. S. Parsi, Considerations of Soil-Structure-Interaction for Seismically Isolated Nuclear Reactor Buildings, *MCEER-24-0003* (University at Buffalo, 2024).

20. Y.-N. Huang, A. S. Whittaker, R. P. Kennedy, and R. L. Mayes, Assessment of Base-Isolated Nuclear Structures for Design and Beyond-Design Basis Earthquake Shaking, *MCEER-09-0008* (University at Buffalo, 2009).

21. Y. N. Huang, A. S. Whittaker, R. P. Kennedy, and R. L. Mayes, "Response of Base-Isolated Nuclear Structures for Design and Beyond-Design Basis Earthquake Shaking," *Earthquake Engineering and Structural Dynamics* 42, no. 3 (2013): 339–356.

22. US Nuclear Regulatory Commission (USNRC), Part 50—Domestic Licensing of Production and Utilization Facilities (Rockville, MD, 2004).

23. US Nuclear Regulatory Commission (USNRC), Part 52—Licenses, Certifications, and Approvals for Nuclear Power Plants (Rockville, MD, 2004).

24. US Nuclear Regulatory Commission (USNRC), Risk-Informed, Technology-Inclusive Regulatory Framework for Advanced Reactors, *Proposed rule (ML21162A102)* (Rockville, MD, 2020).

Appendix 1: An Alternate Approach to Generate a Demand Curve

An alternate approach (A2) to generate a seismic displacement demand curve is presented in this appendix. Approach A2 uses 30 sets of spectrally matched ground motion pairs per bin and explicitly accounts for the dispersion in the displacement demand in the bin, as described below. (The approach presented in the body of the paper, identified as A1 in this appendix, uses analysis of 11 sets of spectrally matched ground motion pairs per bin to estimate a median displacement, and addresses the dispersion in a bin using β_0, equal to 0.28.) Both Approach A1 and Approach A2 use 11 bins or intensity levels for the risk calculations.

In Approach A2, nonlinear dynamic analysis is performed for 30 sets of spectrally matched ground motion pairs in each of the i = 11 bins to generate 330 values of maximum horizontal displacement. These displacements are increased by a factor of 1.2 to address variability in horizontal shaking about the geometric mean and in the mechanical properties of the isolators and dampers: identical to approach A1. The 30 maximum horizontal displacements in the ith bin are assembled in a 30 × 1 vector, D^i, where i = 1 to 11. Vector D^i has 30 entries, d^i_j, organized in increasing order, where j (= 1 to 30) is the ground motion index, and d^i_1 and d^i_{30} are the minimum and maximum displacements in the ith bin. Each bin is associated with a MAF, ΔE^i. Each displacement in the ith bin, d^i_j, is assigned a MAF given by $\Delta E^i_j = \Delta E^i / n_{gm}$, where n_{gm} is the number of ground motion pairs used for analysis in each bin (= 30 here).

The seismic displacement demand curve is defined using 20+ query displacement points, d_{query}, that lie in the range[10] from d^1_{30} to d^{11}_1. The MAFE of exceeding a chosen d_{query} is the sum of the MAFs of all displacements greater than d_{query} in all bins. The query displacements and the corresponding MAFE are used to construct the curve. Figure A1 illustrates the steps involved in approach A2.

Because the demand curve generated using approach A2 directly accounts for the dispersion associated with using spectrally matched horizontal motions, β_0 = 0 in the calculation of β_d per Equation (6). That is,

$$\beta_d = \sqrt{\beta_0^2 + (\beta_{M2}^2 - \beta_{G0}^2) + \beta_r^2 + \beta_m^2 + \beta_f^2}$$

$$= \sqrt{0^2 + (0.14^2) + 0.05^2 + 0.05^2 + 0.05^2} = 0.17$$

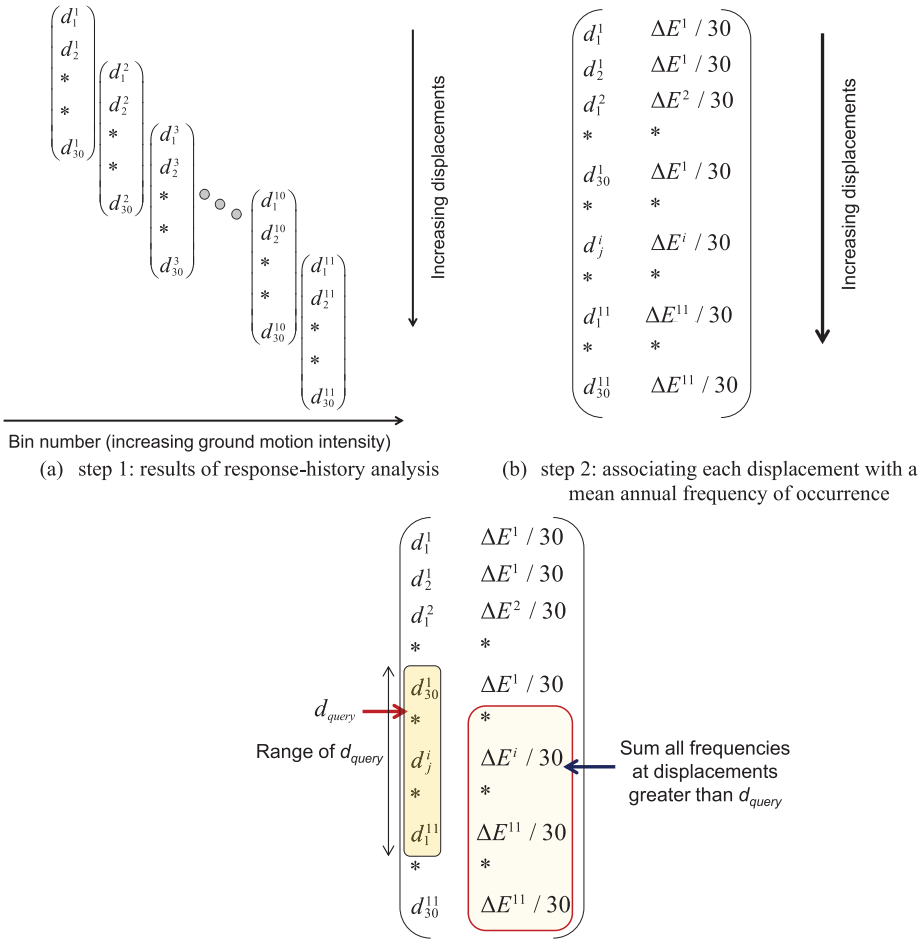

(a) step 1: results of response-history analysis

(b) step 2: associating each displacement with a mean annual frequency of occurrence

FIGURE A1 | Defining a displacement demand curve using results of response-history analysis, Approach A2.

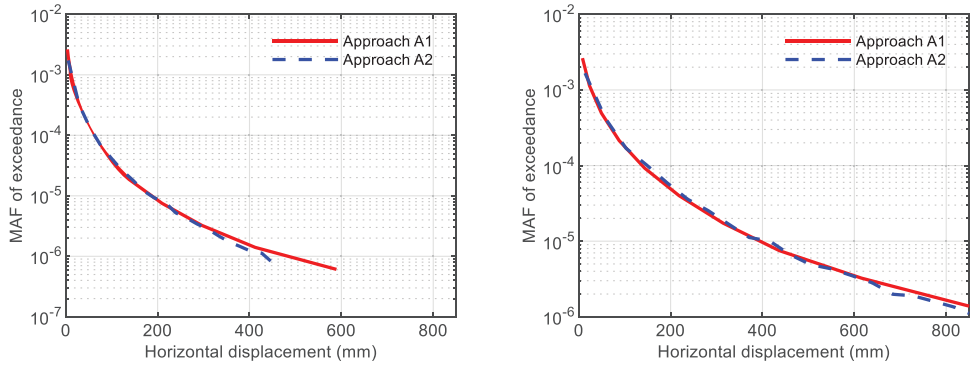

(a) BC soil

(b) CD soil

FIGURE A2 | Comparison of seismic displacement demand curves generated using Approaches A1 and A2, 2-second linear system + nonlinear FVDs, Clinch River site.

Thus, the composite logarithmic standard deviation per Equation (2) for performance calculations using approach A2 is:

$$\beta = \sqrt{\beta_d^2 + \beta_c^2} = \sqrt{0.17^2 + 0.05^2} = 0.18$$

Figure A2 presents displacement demand curves for isolation system 3 (2-s linear system + nonlinear FVDs) generated using Approaches A1 and A2 for BC and CD soils and the Clinch River site. To characterize the difference between the risk numbers determined using Approaches A1 and A2, performance calculations are presented for three isolation systems with median displacement capacities of 200 and 250 mm. Composite logarithmic standard deviations of 0.35 and 0.18 are used for Approaches A1 and A2, respectively[11]. Table A1 presents the corresponding risk numbers, with the approach recommended in the body of the paper (= A1) used as the benchmark. From a seismic PRA perspective, the risk numbers are essentially identical.

TABLE A1 | Performance calculations using two approaches to generate a seismic displacement demand curve, Clinch River, β =0.35 for Approach A1 and = 0.18 for Approach A2.

	Median displacement capacity (mm)	MAF of unacceptable performance		Percent difference
		Approach A1	Approach A2	
(a) BC soil				
2-s linear isolation system	200	6.6×10^{-5}	5.4×10^{-5}	−24
	250	3.7×10^{-5}	2.8×10^{-5}	−32
2-s sliding isolation system	200	1.0×10^{-5}	8.4×10^{-4}	−21
	250	6.5×10^{-6}	5.1×10^{-6}	−27
2-s linear isolation system +. nonlinear FVDs	200	1.1×10^{-5}	8.6×10^{-6}	−26
	250	6.3×10^{-6}	4.6×10^{-6}	−35
(b) CD soil				
2-s linear isolation system	200	2.4×10^{-4}	2.1×10^{-4}	−14
	250	1.5×10^{-4}	1.2×10^{-4}	−21
2-s sliding isolation system	200	5.8×10^{-5}	5.4×10^{-5}	−7
	250	4.0×10^{-5}	3.7×10^{-5}	−7
2-s nonlinear system + nonlinear FVDs	200	2.8×10^{-5}	2.6×10^{-5}	−10
	250	1.9×10^{-5}	1.6×10^{-5}	−13